Lattice dynamics and structural phase transitions in the chain compounds TMMC and TMCC. I. Structural study

1990 J. Phys.: Condens. Matter 2 8209

(http://iopscience.iop.org/0953-8984/2/42/001)

J. Phys.: Condens. Matter **2** (1990) 8209–8228. Printed in the UK

Lattice dynamics and structural phase transitions in the chain compounds TMMC and TMCC: I. Structural study

M N Braud†, M Couzi‡, N B Chanh†, C Courseille†, B Gallois†, C Hauw† and A Meresse†

† Laboratoire de Cristallographie et de Physique Cristalline (URA 144, CNRS), Université de Bordeaux I, 33405 Talence Cédex, France

‡ Laboratoire de Spectroscopie Moléculaire et Cristalline (URA 124, CNRS), Université de Bordeaux I, 33405 Talence Cédex, France

Received 9 March 1990, in final form 30 May 1990

Abstract. The structural phase transitions occurring in the chain compounds $(CH_3)_4NMnCl_3$ (TMMC) and $(CH_3)_4NCdCl_3$ (TMCC) are studied through x-ray diffraction measurements. In both compounds, the existence of a new high-temperature orientationally disordered phase is established (phase I') with space group $P6_3/mmc$ and $Z = 2$ (parent phase). The room-temperature phase I of TMMC and TMCC (space group $P6_3/m$ and $Z = 2$) derives from I' by a rotation of the octahedra chains about the *c* axis; orientational disorder of the $(CH_3)_4N^+$ group (TMA) in phase I is described by a complex Frenkel model involving at least five different orientations of the TMA. Phase II of TMMC (space group $P2_1/b$ with $Z = 4$) is derived from phase I by anti-phase translational displacements of the octahedra chains along the *c* axis; an important amount of residual disorder of the TMA is observed just below the I ↔ II transition temperature. In TMCC, the space group $P2_1/m$ ($Z = 2$) of phase III is confirmed, whereas phase IV exhibits a complex structure (space group $P2_1/b$ with $Z = 12$) corresponding to a trebling of the lattice constant along *c* and a doubling along *b*. X-ray diffuse scattering experiments on TMMC and TMCC are also reported. In phase I, the diffuse scattering patterns are interpreted in terms of 'linear' translational disorder of the octahedra chains along the *c* axis: In phase II of TMMC, a residual translational disorder of the chains is evidenced, just below the I ↔ II transition temperature. These results show that orientational disorder of the TMA group is coupled to translational disorder of the octahedra chain sublattice.

1. Introduction

The crystals with formula $(CH_3)_4NMnCl_3$ (TMMC) and $(CH_3)_4NCdCl_3$ (TMCC) exhibit a one-dimensional type structure, built up from infinite chains made of MCl_6 octahedra sharing opposite faces; the space between chains is occupied by the $(CH_3)_4N^+$ cations (TMA) [1, 2]. TMMC has been widely studied because of its quasi-ideal one-dimensional magnetic properties. In addition, TMMC and TMCC undergo a number of structural phase transitions, governed essentially by the reorientational dynamics of the TMA groups [3–10]. Many problems concerning the structures of the low-temperature ordered phases are still unsolved, so that a model description of the transition mechanism has not been made possible [10].

At ambient pressure, TMMC exhibits at 126 K a first-order structural phase transition from a hexagonal disordered phase (phase I) with space group $P6_3/m$ and $Z = 2$ formula

0953-8984/90/428209 + 20 $03.50

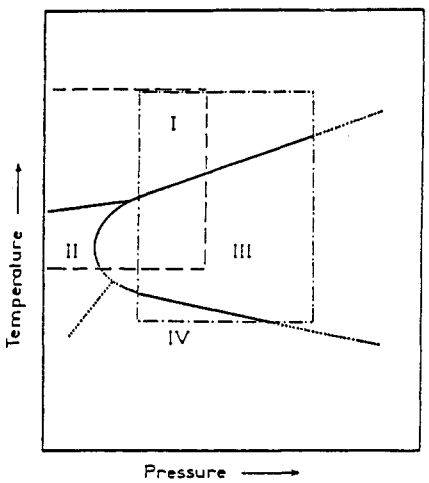

Figure 1. The generalised P, T phase diagram of TMMC and TMCC (after [10]): – – – –, part of the diagram observed with TMMC; – · – · –, part of the diagram observed with TMCC; . . . . . , possible extrapolated transition lines.

units to an ordered monoclinic phase (phase II). Orientational disorder of the TMA groups in phase I arises from the incompatibility of the molecular T_d symmetry with the C_{3h} site symmetry (C_{3h} is not a subgroup of T_d). A model has been proposed to describe the disordered TMA [1], in which one C–N bond lies on the threefold axis of the site, so that the TMA is statistically distributed between two mirror-related (σ_h perpendicular to C_3) equivalent orientations; hereafter, this will be referred to as model (1). More recently, another model has been proposed (model (2)), in which two C–N bonds of the TMA are contained in the σ_h mirror plane, so that the TMA are distributed between three energetically equivalent orientations generated by the threefold axis [11]. The structure of phase II is still the subject of discussion [3, 4, 7–10]. From x-ray diffraction, the space group $P2_1/b$ with $Z = 4$ has been determined, corresponding to a doubling of the lattice constant along $\boldsymbol{b}$ contained in the hexagonal plane [3]. On the other hand, a monoclinic unit cell with $Z = 8$, corresponding to a quadrupling of the lattice period in that direction, has been proposed from neutron diffraction experiments [4]. More recently, phase II was thought to be incommensurate, because of the observation of satellites around the 'forbidden' $00l$ reflections (l odd) on neutron diffraction patterns [9]. Note also that the Raman spectra of phase II would be consistent with the $P2_1/b$, $Z = 4$ space group, provided that cell doubling is due to anti-phase translational displacements of the octahedra chains along the c axis [10].

In the case of TMCC, two successive structural phase transitions have been observed at ambient pressure, at 118 and 104 K, respectively [3, 6–8, 10], both being of first order. The first one (118 K) connects phase I to a monoclinic phase with space group $P2_1/m$ and $Z = 2$ [3] (phase III), and the second one (104 K) leads to another monoclinic phase (phase IV), whose space group is still unknown, and which exhibits a complex structure with at least $Z = 8$ [8].

It should also be pointed out that phase III becomes stable in TMMC at low temperature, under pressure higher than $\simeq 1$ kbar [10]; then, a generalised P–T phase diagram for TMMC and TMCC has been proposed (figure 1), thus suggesting that a unique model may describe all structural phase transitions occurring in these systems [10].

In order to get a better insight into the transition mechanisms of these materials, we have undertaken a systematic study of the structural phase transitions by means of numerous complementary techniques. The results will be presented in a series of three

papers, referred to as I to III, respectively. The present article (I) deals with calorimetric (differential scanning calorimetry (DSC)), x-ray diffraction and diffuse scattering experiments. The experimental details are presented in section 2 and preliminary analysis of the phase transitions in section 3. Sections 4 and 5 are devoted to the structural determination of TMMC in phases I and II, respectively. Finally, x-ray diffuse scattering experiments are reported in section 6. The following articles of this series will be devoted to Raman scattering and ultrasonic measurements (II) and Landau theory of the phase changes (III). A preliminary report of this work has been published elsewhere [12].

2. Experimental details

2.1. Sample preparation

Single crystals of TMMC and TMCC have been prepared by slow evaporation at room temperature of saturated acidic aqueous solutions containing stoichiometric amounts of tetramethylammonium chloride and of manganese or cadmium chloride. Prism-shaped pink (TMMC) and colourless (TMCC) single crystals of good optical quality, elongated along the hexagonal axis, are obtained with dimensions up to $3 \times 3 \times 8\ mm^3$. Small crystals of about $0.8 \times 0.4 \times 0.12\ mm^3$ have been selected for x-ray diffraction measurements, after examination through a polarising microscope.

2.2. DSC measurements

Differential scanning calorimetric (DSC) measurements were performed both on a Dupont de Nemours DSC model 910/990 and a Perkin-Elmer DSC series 7. For the first equipment, the thermal recording conditions were: temperature increasing or decreasing rates of 1 or 2 K min^{-1}, sensitivity of 5000 $\mu V\ mW^{-1}$; the temperature range extends from 93 to 420 K; for all experiments, the powder sample, about 2 mg, was put into hermetically sealed metal capsules. Additional experiments in the high-temperature range (295–450 K) were performed with the second DSC equipment with the following conditions: temperature increasing and decreasing rates of 4 K min^{-1}, sample weight of about 14 mg.

2.3. X-ray diffraction

Powder x-ray diffraction experiments as a function of temperature have been performed with a Guinier–Simon camera from Enraf-Nonius, using the Cu K_α radiation obtained with a quartz monochromator. A powder Secasi counter diffractometer has also been used.

Single crystals of TMMC and TMCC have been studied with Weissenberg and precession cameras, as well as with a four-circle Enraf-Nonius CAD4 diffractometer, using the Mo K_α radiation obtained with a graphite monochromator. Low-temperature measurements down to $\simeq 113$ K were achieved by means of an Enraf-Nonius nitrogen gas flow system. High-temperature measurements up to $\simeq 430$ K have been made with a home-made heating device.

Some experiments at very low temperature, down to $\simeq 10$ K, were performed on a special Weissenberg camera [13] coupled with a Displex CS202 helium gas refrigerator from Air-Products.

2.4. X-ray diffuse scattering

X-ray diffuse scattering experiments have been made on a precession camera that makes it possible to obtain fixed crystal photographs and also to get photographs of selected planes in the reciprocal lattice. The Mo K_α radiation, monochromatised with a graphite crystal, has been used.

Two different crystal orientations have been adopted. In the first one, the $\boldsymbol{b}$ axis (or $\boldsymbol{a}$) is set parallel to the incident x-ray beam, so as observe the planes parallel to ($\boldsymbol{a}^*$, $\boldsymbol{c}^*$) or ($\boldsymbol{b}^*$, $\boldsymbol{c}^*$). In the second one, the $\boldsymbol{c}$ axis is put parallel to the incident beam, thus allowing the observation of the planes parallel to ($\boldsymbol{a}^*$, $\boldsymbol{b}^*$).

The exposure time for fixed-crystal photographs was about two days with a generator power of 1 kW and a crystal of dimension $0.6 \times 0.6 \times 0.8$ mm^3. Precession photographs of different planes $hk0$, $hk1$, $hk2$, . . . were taken with exposure times of about five days.

3. Preliminary analysis of the phase transitions

3.1. DSC experiments

Numerous cycles of heating and cooling between 93 and 420 K always show the presence of thermal accidents related to the first-order I ↔ II transition of TMMC and I ↔ III and III ↔ IV transitions of TMCC reported previously [3–10]. In addition, we have found another thermal anomaly at 389 and 400 K in TMMC and TMCC respectively corresponding to accidents noted previously in the temperature evolution of elastic constants and hypersonic attenuation [14, 15]. A phase change occurring at these temperatures will be confirmed hereafter by x-ray diffraction; the new high-temperature phase is denoted I′. No hysteresis can be detected and the DSC signal exhibits the characteristic shape of a second-order (or nearly second-order) transformation.

3.2. The I′ ↔ I transition

The I′ ↔ I structural phase transition is confirmed to be continuous (or nearly continuous) on Guinier–Simon photographs of TMMC and TMCC. The only detectable change in the diffraction patterns is the disappearance of a weak reflection (111) of TMMC around the transition temperature.

This has been confirmed on Weissenberg photographs; examination of ($hk1$), ($h1l$) or ($1kl$) planes show that reflections of the hhl type with l odd which are present in phase I disappear in phase I′. Then, the space group of phase I′ is unambiguously determined as $P6_3/mmc$ ($Z = 2$), i.e. a supergroup of $P6_3/m$ (phase I), as it should be when the transition I′ ↔ I is found of second-order. Phase I′, of $CsNiCl_3$ type [16], represents the aristotype structure of these systems.

3.3. The I ↔ II transition of TMMC

Guinier–Simon photographs of TMMC through the I ↔ II transition exhibit marked inflections in line positions as well as splitting of several reflections occurring at the transition temperature ($\simeq$126 K); the quasi-continuous thermal evolution is consistent with a weakly first-order phase transition as reported before [9, 17].

Weissenberg and precession photographs of TMMC in phase I confirm the $P6_3/m$ ($Z = 2$) space group [3].

Table 1. Lattice parameters of TMMC in the different phases as determined from single-crystal and powder measurements.

Phases	Type of measurement	T (K)	Parameters (Å) a	b	c	Angle γ (deg)	Volume (Å^3)
I' $P6_3/mmc$ ($Z = 2$)	Single-crystal (precession)	423	9.25		6.53	120	483.9
	Powder (Guinier–Simon)	443	9.234(4)		6.516(5)	120	481.2(8)
I $P6_3/m$ ($Z = 2$)	Single-crystal (Weissenberg)	293	9.12		6.49	120	467.5
	Single-crystal (CAD4)	293	9.145(3)		6.491(3)	120	470.1(5)
		195	9.098(5)		6.475(5)	120	464.2(9)
		150	9.067(5)		6.477(5)	120	461.1(9)
	Powder (diffractometer)	293	9.151(1)		6.490(1)	120	470.7 (2)
II $P2_1/b$ ($Z = 4$)	Single-crystal (Weissenberg)	118	9.03	18.35	6.46	120.5	922.3
	Single-crystal (CAD4)	118	9.051(2)	18.107(4)	6.476(2)	120.01(2)	919(11)
	Powder (Guinier–Simon)	115	9.018(3)	18.343(4)	6.442(3)	120.71(2)	916(12)

In phase II (113 K), Weissenberg photographs of the $hk0$ and $hk1$ planes have been obtained, as well as a precession photograph of the $0kl$ plane. On the $hk1$ plane, superstructure reflections are observed along $\boldsymbol{a}^*$ and $\boldsymbol{b}^*$, which were absent in phase I. In contrast, the $hk0$ plane is exempt of superstructure reflection, which implies an extinction condition for $hk0$ reflections with h or k odd. Also, as in phase I, we notice the systematic absence of $00l$ (l odd) reflections in the $0kl$ plane.

On the other hand, the main reflections, which are unique in phase I, are split into three components in phase II; this comes from the existence of ferroelastic domains in phase II such that the $\boldsymbol{c}$ axis is conserved. Because of these domains, we can explain the fact that superstructure reflections are present in both the $\boldsymbol{a}^*$ and $\boldsymbol{b}^*$ directions, but that cell doubling occurs in one of these directions only.

Thus, the space group of phase II is deduced from that of phase I by a doubling of one hexagonal parameter $\boldsymbol{a}_I$ or $\boldsymbol{b}_I$, which leads to a monoclinic structure with space group $P2_1/b$ with $Z = 4$ (doubling along $\boldsymbol{b}$) and with lattice parameters such as $a_{II} \simeq a_I$, $b_{II} \simeq 2b_I$, $c_{II} \simeq c_I$; the monoclinic angle is $\gamma \simeq 120°$.

So, our results are in full agreement with a previous x-ray diffraction study [3]. Even by taking very long exposure times, we were not able to observe the 'forbidden' $00l$ (l odd) reflections, nor the associated satellites, as reported from neutron diffraction measurements [9]. It should be noticed that the latter experiments have been carried out on a deuterated d-TMMC sample, doped with Ni, even though the phenomenon seems to be present in the pure d-TMMC in the whole domain of existence of phase II [9]. We believe that the observation of satellites very close to a main Bragg peak may be due to an experimental artefact connected with the domain structure of phase II, as evidenced above, but we have no explanation for the occurrence of $00l$ (l odd) reflections on neutron diffraction patterns. Perhaps, we can consider that the structure of d-TMMC is different from that of the hydrogenated homologue, and/or that particular phenomena

Table 2. Lattice parameters of TMCC in the different phases as determined from single-crystal and powder measurements.

Phases	Type of measurement	T (K)	Parameters (Å) a	b	c	Angle γ (deg)	Volume (Å^3)
I' $P6_3/mmc$ ($Z = 2$)	Powder (Guinier–Simon)	443	9.235(4)		6.742(5)	120	498.0(8)
I $P6_3/m$ ($Z = 2$)	Single-crystal (Weissenberg)	293	9.11		6.73	120	483.7
	Powder (diffractometer)	293	9.139(1)		6.723(1)	120	486.3(2)
III $P2_1/m$ ($Z = 2$)	Single-crystal (Weissenberg)	115	9.33	8.76	6.67	120.5	469.7
	Powder (Guinier–Simon)	115	9.326(3)	8.809(3)	6.683(2)	120.97(2)	471(6)
IV $P2_1/b$ ($Z = 12$)	Single-crystal (Weissenberg)	100	8.84	18.41	20.0	120.5	
		45	8.79	18.43	20.1	120.5	2804.5
	Powder (Guinier–Simon)	105	8.852(7)	18.45(2)	20.09(2)	121.08(6)	2805.6
							2810 (100)

related to the ordering of the CH_3 (CD_3) groups are observed with neutron diffraction but cannot be evidenced by x-rays [9].

In the absence of further information, we shall consider in the following that the space group of phase II is $P2_1/b$ ($Z = 4$), which anyway represents the main lattice, knowing that an additional distortion may eventually be present. In table 1, we have summarised our data concerning the unit-cell determinations of TMMC in phases I', I and II.

3.4. The I ↔ III ↔ IV phase sequence of TMCC

The space groups $P6_3/m$ ($Z = 2$) and $P2_1/m$ ($Z = 2$) are confirmed for phase I and III of TMCC, respectively. On the Weissenberg photographs of the $hk0$ and $hk1$ planes in phase III (115 K), no superstructure reflection is noticed, but again we find the three types of domains characteristic of the ferroelastic I ↔ III phase transition.

Phase IV of TMCC has been studied with the low-temperature helium device. Bragg photographs at 35 K, with crystal rotating about the $\boldsymbol{c}$ axis, clearly show a trebling of the lattice parameter along $\boldsymbol{c}$, as evidenced by the presence of superstructure reflections along $\boldsymbol{c}^*$, which were not present in phase III nor in phase I. The Weissenberg photograph of the $hk0$ plane at the same temperature is exempt of superstructure reflection, but that of the plane $hk1$ shows new reflections characteristic of cell doubling along $\boldsymbol{a}$ or $\boldsymbol{b}$, similar to those found already in phase II of TMMC. Thus, the space group of phase IV is $P2_1/b$ with $Z = 12$, with lattice parameters such as $a_{IV} \simeq a_I$, $b_{IV} \simeq 2b_I$, $c_{IV} = 3c_I$ and $\gamma_{IV} \simeq 120°$.

In table 2, we have summarized our data concerning the unit-cell determinations of TMCC in phases I', I, III and IV. The lattice parameters determined in phase III are somewhat different from those reported previously [3].

4. The crystal structure of TMMC in phase I

As mentioned already, the TMA group in phase I exhibits orientational disorder whose nature is still not well established [3, 11, 18]. In fact, the determination of a model description for the orientational disorder is of major importance in the comprehension of transition mechanisms; in the case of TMMC and TMCC, the important question is to know to what extent the TMA disorder pertains to model (1) [1, 2, 11], model (2) [11, 18] or to another type. In order to go through this problem, we have determined the structure of phase I of TMMC at different temperatures.

The x-ray reflections have been collected on a CAD4 diffractometer at three selected temperatures (293, 195 and 150 K), using the Mo K_α radiation ($\lambda = 0.71069$ Å). An ω–2θ scan was used. The structure search was based on the heavy-atom method, and refinements were made by a least-squares process using the SHELX program system [19]. The scattering factor of Mn atom has been taken from [20], all other factors, corresponding to Cl, N and C atoms, already being included in SHELX.

First, the Mn atoms are put in sites 2(b) (0, 0, 0), the nitrogen in site 2(d) (1/3, 2/3, 1/4) and the chlorine in 6(h) (x, y, 1/4); the starting coordinates x and y of Cl atoms are those determined previously by Morosin and Graeber [1]. After refinement only with these Mn, N and Cl atoms, the atomic positions remain essentially unchanged and the reliability factors obtained ($R \simeq 0.09$, $R_w \simeq 0.11$)† show that the contribution of the CH_3 groups to the diffracted intensities is rather small, as expected.

Now, examination of Fourier difference maps reveals electronic density residues around the nitrogen atom, corresponding to the CH_3 groups. They are in the shape of three semi-circular arcs joining together on the threefold axis (figure 2). The electronic density is not homogeneous inside each semi-circle; at room temperature it is rather spread out but exhibits a maximum (1.12 e^-) on the mirror plane of the site, at $z/c = 0.25$, then decreases to a minimum (0.43 e^-) at $z/c = 0.44$ (0.06) and again shows a maximum (0.75 e^-) on the threefold axis, at $z/c = 0.48$ (0.02) (figure 2). At low temperatures (195 and 150 K), the positions of carbon atoms are more precisely defined, as shown by an increase of the electronic densities on the mentioned sites (figure 2).

Clearly, neither model (1) (absence of carbon atom on the mirror plane) nor model (2) (absence of carbon atom on the threefold axis) is able to account for the experimental observation. Thus, we are led to consider a combination of the two models; indeed, in the simple hypothesis of equal contributions of models (1) and (2), the distribution of electronic density calculated with such a Frenkel model (finite number of discrete orientations) is in qualitative agreement with the experimental ones (figures 2 and 3). However, the observed values of electronic density maxima are always lower than calculated, which means that the different potential wells of the TMA are not precisely located, probably because of fluctuations of the crystal lattice (see section 6); nevertheless, the Frenkel-type description will be adopted as a reasonable approximation.

Then, the structure refinement is carried on, with the TMA considered as rigid bodies with tetrahedral symmetry, as supported by the Raman data obtained in phase I [7]; thus, C–N and C–C distances are fixed on standard values, i.e. 1.479 and 2.415 Å respectively. The proportions p_1 or p_2 of model (1) or model (2) ($p_1 + p_2 = 1$) are

† The reliability factor R is defined as $R = \Sigma||F_o| - |F_c||/\Sigma|F_o|$ where F_c and F_e are the observed and calculated structure factors, respectively. According to the weighting scheme of the SHELX program the weight w of a given reflection is $w = k/\sigma^2(F_o) + |g|/F_0^2$ (k must be close to 1 if there is no systematic error). Then, the weighted reliability factor R_w is defined as $R_w = \Sigma(||F_o| - |F_e||\sqrt{w})/\Sigma(F_o\sqrt{w})$.

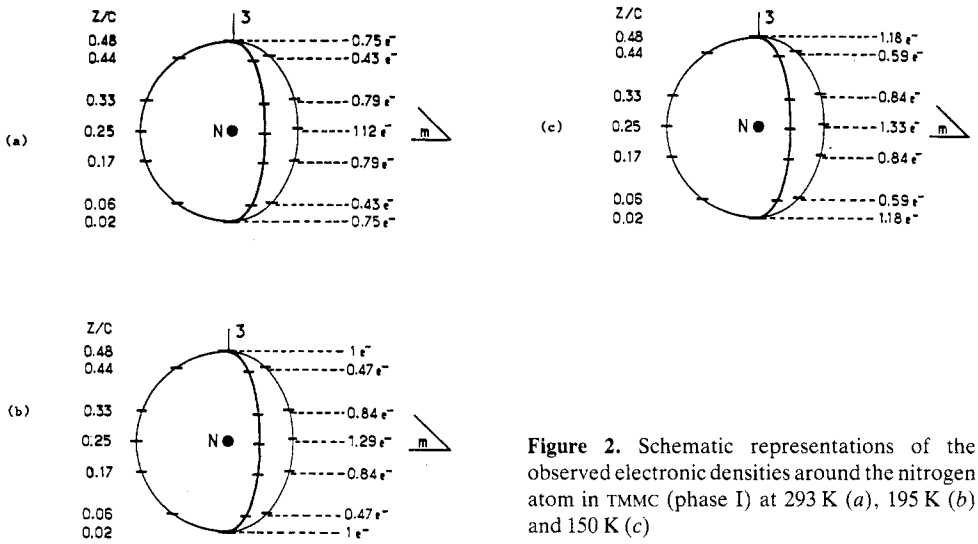

Figure 2. Schematic representations of the observed electronic densities around the nitrogen atom in TMMC (phase I) at 293 K (*a*), 195 K (*b*) and 150 K (*c*)

adjusted so as to give the best reliability factor. A schematic representation of the structure of phase I determined in such a way is given in figure 4. The final positional parameters (293 K) are given in table 3 and the anisotropic thermal factors of Mn, Cl and N atoms in table 4. Selected interatomic distances and angles are reported in table 5 and the values of p_1 and p_2, together with the best reliability factors, are indicated in table 6. Given the approximations introduced in the structure determination and the important uncertainties on the carbon positions, it is not meaningful to discuss possible variations of p_1 or p_2 as a function of temperature; nevertheless, we may conclude that

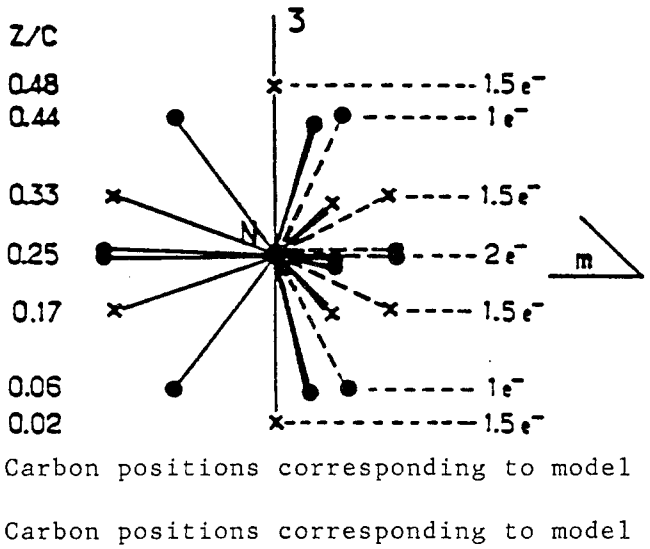

Figure 3. Calculated electronic densities around the nitrogen atom for a combination of model (1) and model (2) with $p_1 = p_2 = 0.5$ (see text): ×, carbon positions corresponding to model (1); ●, carbon positions corresponding to model (2).

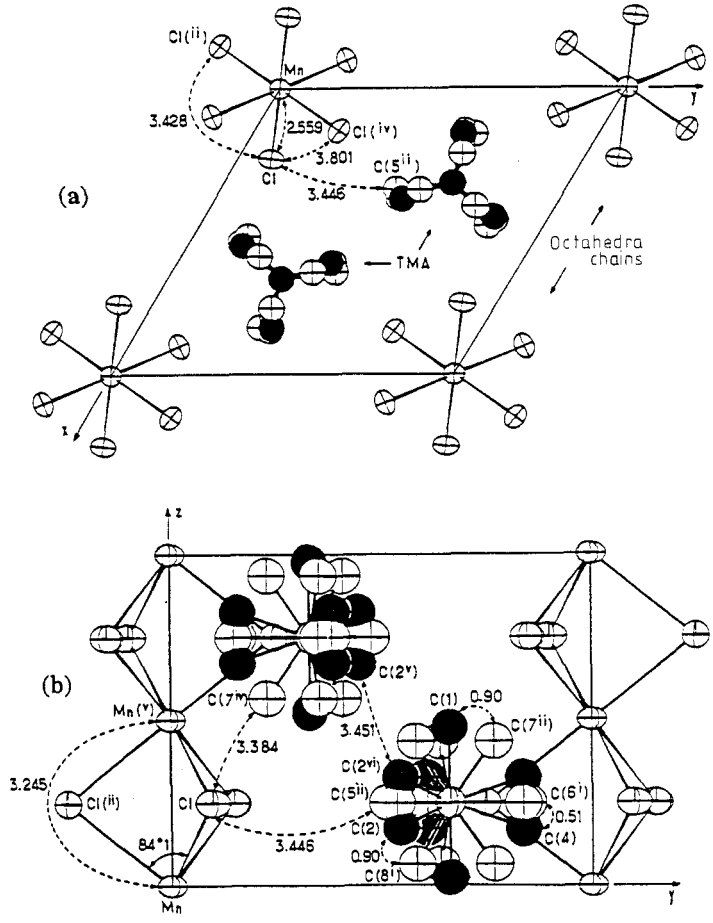

Figure 4. Schematic representations of the structure of phase I of TMMC at 293 K: (*a*) projection in the (001) plane; (*b*) projection in the (100) plane; ●, carbon atoms pertaining to model (1); +, carbon atoms pertaining to model (2).

relative contributions of model (1) and model (2) to the TMA orientational disorder are roughly equal, i.e. $p_1 \simeq p_2 \simeq 0.5$ (table 6).

4.1. Remarks on the structure of phase I'

Group subgroup relation connects phase I ($P6_3/m$) to phase I' ($P6_3/mmc$). Because of the appearance of vertical (σ_V) mirror planes in phase I', some differences in atomic positions may be expected, with respect to those given in table 3 for phase I:

(i) The chlorine atoms must be situated in positions 6(h) (x, $2x$, 1/4), which means that the $MnCl_3$ octahedra chains should execute a rotational motion about their long axis (*c* direction) when going from phase I to phase I'.

(ii) The TMA groups must be in positions 2(c) (1/3, 2/3, 1/4) in a site of symmetry D_{3h} ($\bar{6}m2$). Using the Frenkel description given above for phase I, all atomic positions of the carbon derived from model (1) and model (2) must be split into two equivalent

Table 3. Final positional parameters and equivalent isotropic thermal factors ($B_{eq} = (4/3)\Sigma\Sigma\, b_{ij}a_ia_j$) for phase I of TMMC at 293 K.

	Atoms	x/a ($\times 10^4$)	y/b ($\times 10^4$)	z/c ($\times 10^4$)	B_{eq}
	Mn	0	0	0	2.2(1)
	Cl	2481(1)	984(1)	2500	2.8(1)
	N	3333	6666	2500	2.9(2)
Model (1)	C(1)	3333	6667	4775(6)	6.0(5)
	C(2)	3877(23)	5488(19)	1732(14)	6.0(5)
	C(3)	1611(9)	6122(23)	1732(14)	6.0(5)
	C(4)	4510(19)	8387(9)	1731(14)	6.0(5)
Model (2)	C(5)	4830(20)	8378(14)	2500	3.4(8)
	C(6)	3880(31)	5391(24)	2500	3.4(8)
	C(7)	2301(14)	6439(20)	4356(16)	3.4(8)
	C(8)	2305(14)	6440(20)	639(16)	3.4(8)

Table 4. Anisotropic thermal factors for phase I of TMMC at 293 K. The temperature factors have the form: $\exp[-(\beta_{11}h^2 + \beta_{22}k^2 + \beta_{33}l^2 + \beta_{12}hk + \beta_{13}hl + \beta_{23}kl)]$.

Atoms	β_{11} ($\times 10^4$)	β_{22} ($\times 10^4$)	β_{33} ($\times 10^4$)	β_{12} ($\times 10^4$)	β_{13} ($\times 10^4$)	β_{23} ($\times 10^4$)
Mn	103(2)	103(2)	92(3)	103(2)	0	0
Cl	89(2)	148(2)	137(3)	104(4)	0	0
N	98(5)	98(5)	175(14)	98(5)	0	0

Table 5. Selected inter-atomic distance (Å) and angles (deg) in phase I of TMMC at 293 K. Standard deviations in the least significant figures are given in parentheses.

Distances (Å)	
Mn–Mn(^{v})	3.245
Mn–Cl	2.559(3)
Cl–Cl(^{ii})	3.428
Cl–Cl(^{iv})	3.801
Cl–C(7^{iv})	3.384(3)
Cl–C(5^{ii})	3.446(3)
Cl–C(6^{i})	3.665(3)
C(2^{vi})–C(2^{v})	3.451(3)
C(1)–C(7^{ii})	0.90(2)
C(2)–C(8^{i})	0.90(2)
C(4)–C(6^{i})	0.51(1)
Angles (deg)	
Cl–Mn–Cl(^{ii})	84.1

Symmetry codes:
(^{i}) $y, x-y, z$
(^{ii}) $y-x, x, z$
(^{iii}) x, y, z
(^{iv}) $x-y, x, z$
(^{v}) $x, y, 1/2+z$
(^{vi}) $x, y, 1/2-z$

Table 6. Result of structure refinements and the corresponding p_1 and p_2 values (see text) for TMMC in phase I at different temperatures.

		$T = 293$ K	$T = 195$ K	$T = 150$ K
Without methyl group	R	0.093	0.094	0.121
	R_w	0.103	0.107	0.14
Including methyl groups	R	0.040	0.036	0.061
	R_w	0.046	0.053	0.078
	p_1	0.64 ± 0.1	0.55 ± 0.1	0.65 ± 0.1
	p_2	0.36 ± 0.1	0.45 ± 0.1	0.35 ± 0.1

positions, related to each other by the additional mirror plane existing in phase I'. Thus, twice as much orientations are accessible to the TMA in phase I', compared to phase I.

5. The crystal structure of TMMC in phase II

Attempts to determine the structure of TMMC in phase II have been made at 118 K, the lowest temperature accessible to the cooling system when adapted on the CAD4 diffractometer. Again, the Mo K_α radiation and ω–2θ scans were used.

As mentioned already, ferroelastic domains exist in phase II and as a result there is a trebling of the main structure reflections. Unfortunately, the scanning of the detector is not able to separate each individual reflection, because at 118 K the departure from hexagonal symmetry is too small; under these conditions, the measured intensities for the main structure reflections represent the addition of three reflections with different *hkl* Miller index (figure 5). In contrast, the superstructure reflections of the different domains are not superimposed (figure 5).

In a first step, the data collection has been performed in a classical way, on the basis of the lattice parameters given in table 2. Under these conditions a number of superstructure reflections were missing, because of their low intensities compared to those of the main reflections. Then, another set of data has been collected, by doubling artificially the lattice parameters in both ***a*** and ***b*** directions so as to measure all superstructure reflections belonging to the three domains; in order not to measure again the very strong main structure reflections, the h and k Miller index were set to odd values only. The superstructure reflections of each domain have been identified and by comparing their intensities it appears that the relative weight of each domain in the crystal is approximately 1/3, as expected when the crystal is not submitted to stress.

The analysis of the Patterson function obtained with the different sets of superstructure reflections confirms the space group $P2_1/b$ and also gives the positions of the Mn and Cl atoms. The Mn atoms are no longer situated on inversion centres at $z/c = 0$, but are displaced by $\simeq 0.03$ Å along the ***c*** direction, carrying away the Cl atoms of the chain in the same direction. This result confirms the mechanism inferred from Raman data, according to which the I ↔ II transition involves antiparallel translational displacements of the octahedra chains along ***c*** [10]. After refinement on the superstructure intensities, a reliability factor of poor quality is obtained ($R = 0.24$), which makes elusive any attempt to solve completely the structure of phase II with the help of superstructure reflections only.

Thus, the main lattice reflections have been added to the data set. After numerous

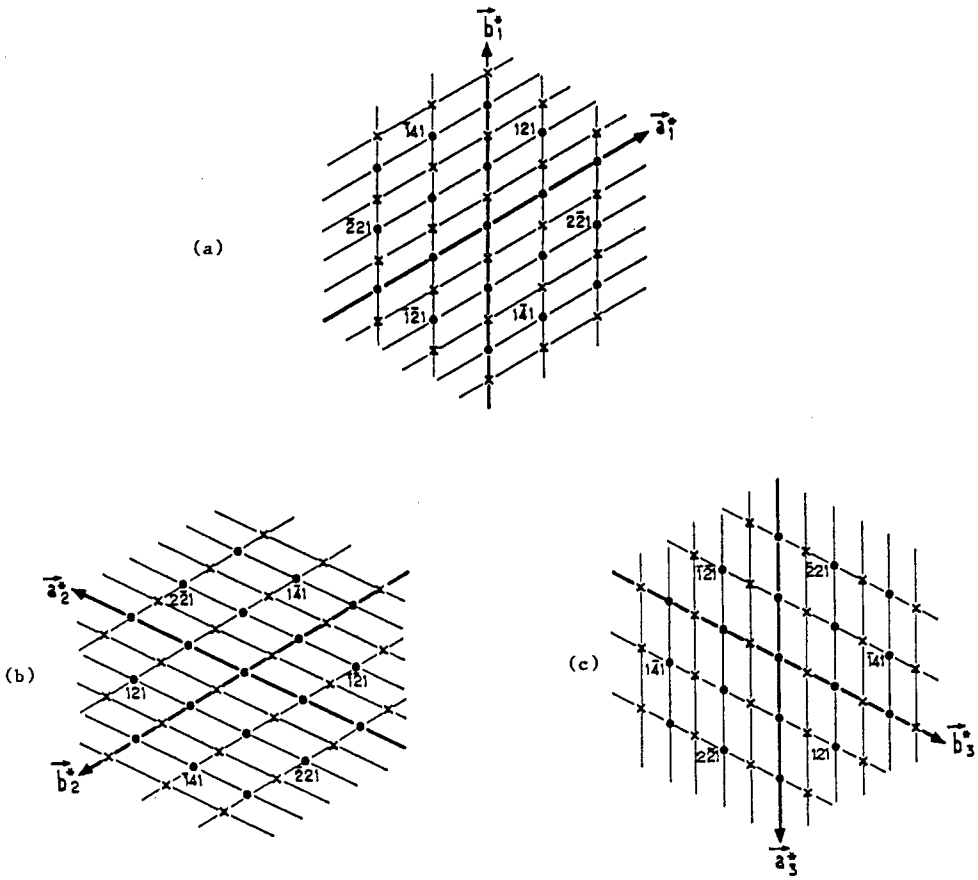

Figure 5. Superposition of the reciprocal lattices of the three domains in phase II of TMMC: (*a*) *hk*1 plane of domain (1); (*b*) *hk*1 plane of domain (2); (*c*) *hk*1 plane of domain (3); ●, main structure reflections; ×, superstructure reflections.

refinements made to take account of the domain structure of the crystal, it turned out that the best reliability factors (obtained without introducing the methyl group) for the main reflections ($R = 0.124$) and for the superstructure reflections ($R = 0.242$) are both obtained when the relative proportion of each domain is set equal to 1/3 and when the structure factors calculated for the superimposed main reflections are quasi-identical. So, we have used the SHELX program in the approximation where the measured intensity of a main reflection is the sum of three equivalent intensities. After refinement of the positions of Mn and Cl atoms given by the Patterson functions, the position of nitrogen is found on Fourier difference maps; further refinements without the methyl groups give an acceptable reliability factor $R = 0.11$. The results are summarised in tables 7 and 8.

Then, the positions of carbon atoms are deduced from Fourier difference maps; in fact, though the structure is monoclinic at 118 K, the same anisotropic semi-circular distributions as those found in phase I are observed, with no detectable departure from hexagonal symmetry. We conclude that an important residual orientational disorder of the TMA is still present at 118 K, i.e. just below the I ↔ II transition temperature (126 K), but that experimental uncertainties prevent any further discussion on the type of ordering

Table 7. Final positional parameters and equivalent isotropic thermal factors ($B_{eq} = (4/3)\Sigma\Sigma\, b_{ij}a_ia_j$) for phase II of TMMC at 118 K.

Atoms	x/a ($\times 10^4$)	y/b ($\times 10^4$)	z/c ($\times 10^4$)	B_{eq}
Mn	0	2500	−44(6)	1.75(2)
Cl(1)	2490(5)	2958(2)	2451(10)	2.08(4)
Cl(2)	−914(5)	3287(2)	2461(10)	2.10(4)
Cl(3)	−1576(5)	1255(2)	2453(10)	2.07(4)
N	3335(17)	5830(8)	2494(37)	2.0(1)

Table 8. Anisotropic thermal factors for phase II of TMMC at 118 K. The temperature factors have the form: $\exp[-(\beta_{11}h^2 + \beta_{22}k^2 + \beta_{33}l^2 + \beta_{12}hk + \beta_{13}hl + \beta_{23}kl)]$.

Atoms	β_{11} ($\times 10^4$)	β_{22} ($\times 10^4$)	β_{33} ($\times 10^4$)	β_{12} ($\times 10^4$)	β_{13} ($\times 10^4$)	β_{23} ($\times 10^4$)
Mn	84(4)	15(1)	71(4)	32(2)	2(1)	−1(1)
Cl(1)	82(5)	22(1)	94(8)	37(4)	−12(5)	−0.5(2)
Cl(2)	109(6)	20(1)	98(8)	53(5)	5(2)	2(1)
Cl(3)	98(6)	16(1)	97(8)	26(4)	−5(2)	2(1)
N	83(20)	18(5)	128(32)	34(16)	−24(10)	−6(2)

that could be expected in phase II at low temperature. We shall return to this point in paper III; clearly, measurements at much lower temperatures would be necessary to solve this problem. As an indication, note that the reliability factor is lowered to $R = 0.06$ when the methyl groups are introduced with the same model of disorder as that adopted in phase I, but again, this has no physical meaning since phase II is monoclinic.

6. X-ray diffuse scattering

In order to establish whether or not the orientational disorder of the TMA is coupled with some kind of disorder due to the octahedra chains [7–10], we have undertaken x-ray diffuse scattering experiments on TMMC and TMCC in phase I at different temperatures and in TMMC in phase II at low temperature. In the hypothesis of existence of chain disorder, x-ray diffuse scattering is of particular interest, because of the strong difference between the scattering factors of the TMA and of the $MnCl_3$ or $CdCl_3$ chains, in favour of these latter. A similar situation has been encountered in the layer-type compounds $(CH_3NH_3)_2CdCl_4$ [21] and $NH_3(CH_2)_5NH_3CdCl_4$ [22], where diffuse streaks characteristic of 'planar disorder' have been observed; in the case of TMMC and TMCC, one would rather expect the occurrence of a diffuse plane, because of the strong unidimensional character of these materials.

6.1. Results

Fixed-crystal photographs of the $(\boldsymbol{a}^*, \boldsymbol{c}^*)$ or $(\boldsymbol{b}^*, \boldsymbol{c}^*)$ reciprocal planes have been obtained at room temperature with TMMC (figure 6(*a*)) and TMCC (figure 6(*b*)). One notices the presence of diffuse planes perpendicular to $\boldsymbol{c}^*$, exhibiting marked modulations; the diffuse scattering patterns indeed correspond to diffuse planes, because they do not depend on the orientation of the crystal around the $\boldsymbol{c}$ axis. The diffuse planes are

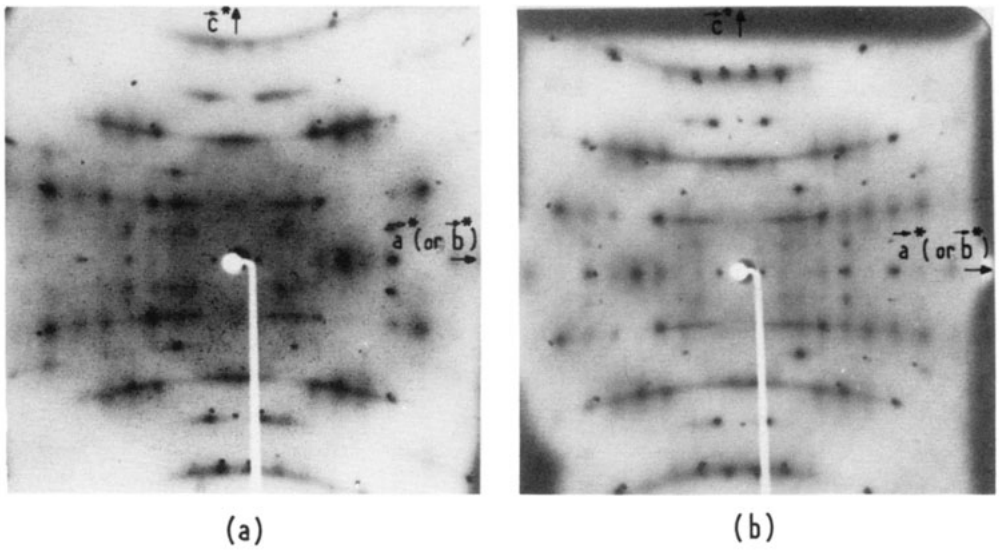

Figure 6. Fixed-crystal photographs of the (a^*, c^*) or (b^*, c^*) plane in phase I of TMMC (*a*) and TMCC (*b*) at room temperature.

superimposed on Bragg peaks, at integer values of the Miller index l; except for the $l = 0$ plane, which is apparently exempt of diffuse scattering phenomenon, the diffuse intensities in those planes with even l index values are much stronger than those with odd l index values (figure 6). In the case of TMCC, where the diffuse scattering patterns are stronger compared to TMMC, a fixed-crystal photograph with long exposure time (seven days) has been made, which confirms the absence of scattering in the $l = 0$ plane (figure 6(*b*)).

The other diffuse planes parallel to (a^*, b^*), i.e. the ($hk1$), ($hk2$), ($hk3$) and ($hk4$) diffuse planes, have been analysed separately by means of precession camera measurements (figures 7(*a*)–(*d*)). In addition to the Bragg peaks, one notices the presence of an inhomogeneous diffuse scattering in the shape of honeycombs, thus showing that the interrupted diffuse planes seen in figure 6 correspond to the intersections of modulated planes with the Ewald sphere. As mentioned above, the diffuse intensity in the ($hk2$) and ($hk4$) planes is much stronger than that observed in ($hk1$) and ($hk3$) (figure 7).

6.2. Discussion

The diffuse scattering patterns observed at room temperature in TMMC and TMCC are quite similar. Then, we shall focus the discussion on TMMC for which precise structural information is known (see sections 4 and 5).

From a general point of view, one notices that the most intense diffuse scattering and diffraction (Bragg peaks) patterns are located at the same places in reciprocal space (figure 7), which probably means that Mn and Cl atoms are responsible for most of the scattering and diffraction processes, since they have much stronger scattering factors than C and H atoms. As a consequence, the observed diffuse planes are assigned essentially to 'linear' disorder [23] coming from the octahedra chains.

A simple model of 'idealised' linear chains made of Mn and Cl_3 atoms randomly

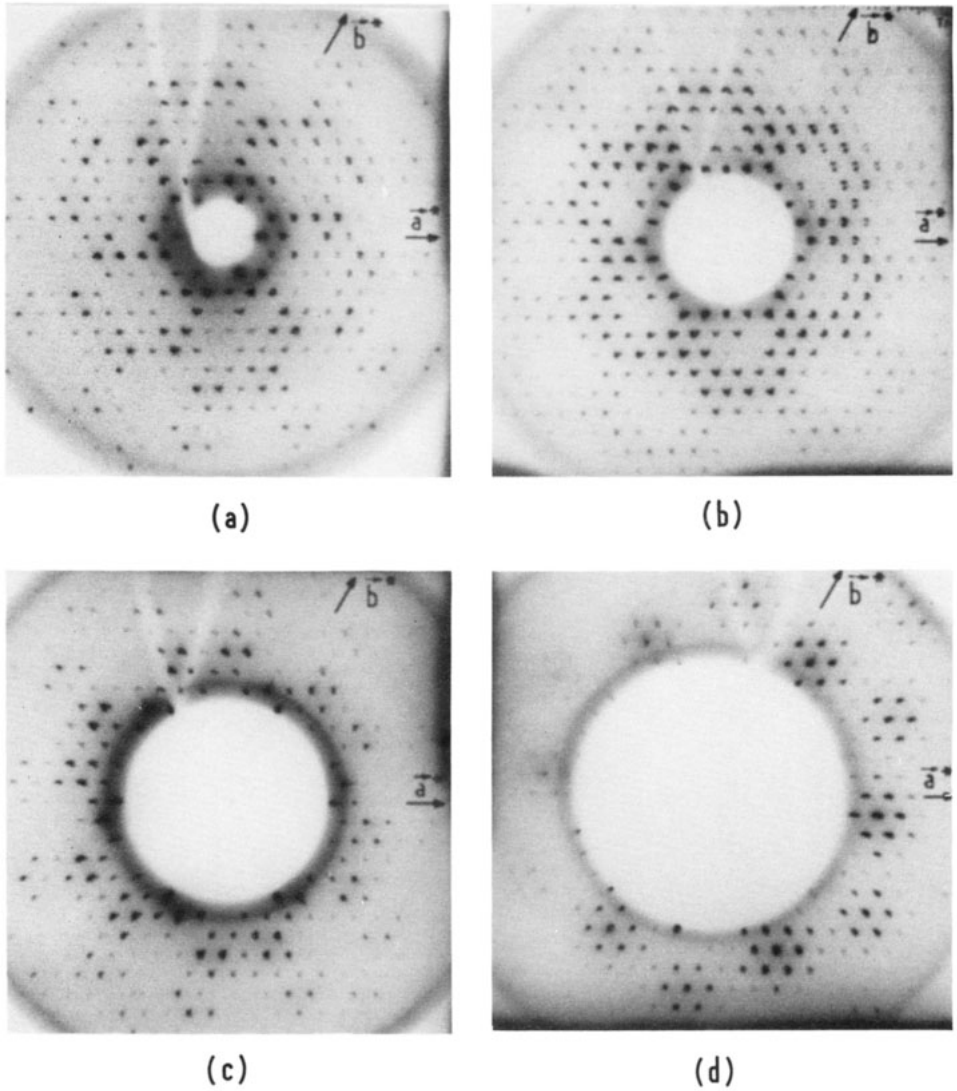

Figure 7. Precession photographs of the ($hk1$) (a), ($hk2$) (b), ($hk3$) (c) and ($hk4$) (d) reciprocal planes of TMMC in phase I at room temperature.

shifted by quantities $+\delta z$ and $-\delta z$ [24] shows that except for the $l = 0$ plane, which is exempt of diffuse scattering, only planes with even values of the Miller index l will exhibit diffuse scattering with an alternation of strong ($l = 4n + 4$) and weak ($l = 4n + 2$) intensities. So, this simple model is able already to account for the gross diffuse scattering patterns. However, we are still left with the presence of modulated diffuse planes and with diffuse scattering corresponding to odd l planes.

6.2.1. The shape factor. The modulation of the diffuse intensity within the different diffuse planes evidenced experimentally (figure 7) may be due to a 'shape factor' of the

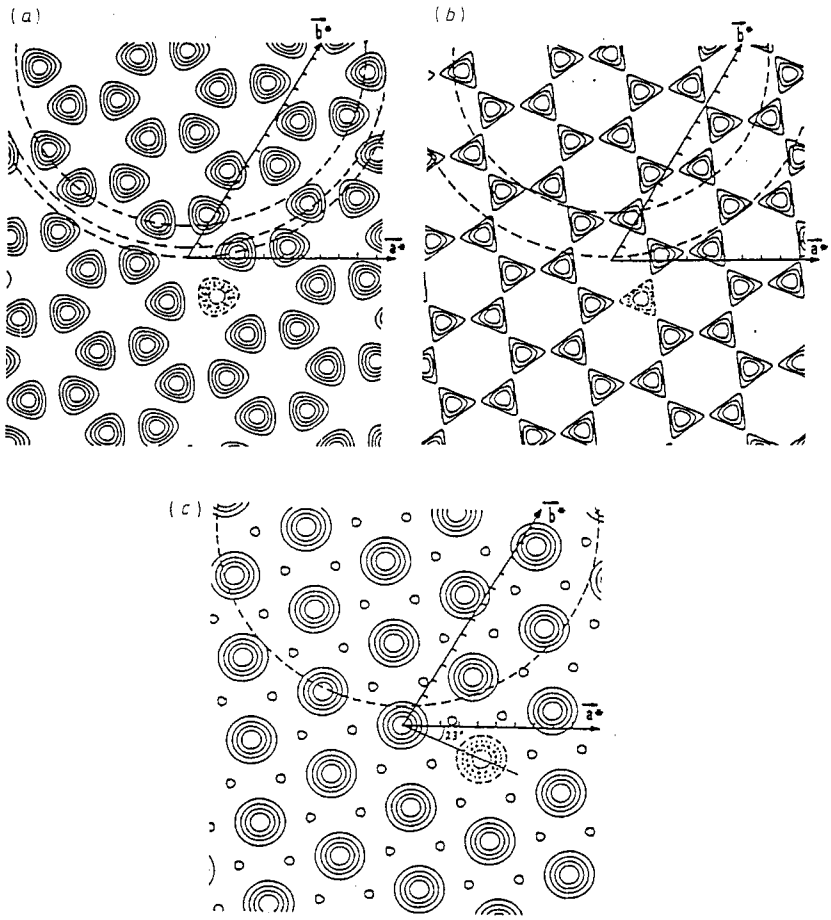

Figure 8. Calculated modulation of the diffuse scattering in the (*hkl*) reciprocal planes, according to the 'shape' factor of the octahedra chains (see text). (*a*) $l = 4n + 1$ and $l = 4n + 3$. Isocline lines corresponding to 20%, 40%, 60% and 80% of $I_{hk}^{max(1)}$ are represented. Broken circular lines correspond to the intersection of the Ewald sphere with the (*hk*5), (*hk*3) and (*hk*1) planes (from up to down) in fixed-crystal photographs. (*b*) $l = 4n + 2$. Isocline lines corresponding to 70%, 80% and 90% of $I_{hk}^{max(2)}$ are represented. Broken circular lines correspond to the intersection of the Ewald sphere with the (*hk*6) and (*hk*2) planes (from up to down) in fixed-crystal photographs. (*c*) $l = 4n + 4$. Isocline lines corresponding to 20%, 40%, 60% and 80% of $I_{hk}^{max(3)}$ are represented. Broken circular line corresponds to the intersection of the Ewald sphere with the (*hk*4) plane in fixed-crystal photographs.

octahedra chains, arising from the fact that these chains exhibit finite lateral dimensions. In order to verify this hypothesis, we have calculated the local structure factor by taking account of the particular positions of the Cl atoms and assuming again that no correlation exists between chains.

The results are shown in figure 8. There is a good agreement between the observed (figure 7) and calculated distributions of diffuse intensity in the (*hk*1), (*hk*2), (*hk*3) and (*hk*4) reciprocal planes. One notices the same modulation period in each plane, extending over 4.5 reciprocal unit cells approximately and directed at about 23° from

the $\boldsymbol{a}^*$ and $\boldsymbol{b}^*$ axes (figure 7). The modulation is related to the geometry of the octahedra chain, which exhibits a finite 'radius' of about 1.98 Å; the ratio of the unit-cell parameter versus chain 'radius' (9.15/1.98 = 4.62) explains the measured modulation period. On the other hand, the angle of 23.2° between the Mn–Cl bonds and the $\boldsymbol{a}$ and the $\boldsymbol{b}$ axis (section 4) is directly related to the modulation direction. Furthermore the intersections of the calculated modulated diffuse planes with the Ewald sphere in ($\boldsymbol{a}^*$, $\boldsymbol{c}^*$) or ($\boldsymbol{b}^*$, $\boldsymbol{c}^*$) fixed crystal photographs reproduce the experimental diffuse scattering patterns of figure 6. Thus, we conclude that the modulation of observed diffuse planes is mainly due to the 'shape factor' of the octahedra chains.

6.2.2. The average structure factor of the chain. In order to account for the presence of diffuse scattering on odd l planes (this was not accounted for by the idealised chain model) together with the absence of scattering on the $l = 0$ plane, we have performed the full calculation of the average structure factor of the real chain.

Using a classical procedure [25] adapted to the symmetry of the octahedra chains as found in TMMC, and assuming again that atomic displacements only occur along the $\boldsymbol{c}$ axis with no correlation between chains, expressions have been established for the amplitude of radiations scattered by the Mn and Cl atoms [24].

From this calculation, it follows that, except for the ($hk0$) plane, which contains only Bragg peaks, all reciprocal planes (hkl) with even and odd l index values will exhibit diffuse scattering; even l planes are expected to show stronger diffuse intensities (both Mn and Cl atoms will contribute to their intensity) than odd l planes (only the Cl atoms will contribute to their intensity). This is in full agreement with the experimental data (figures 6 and 7).

Similar calculations of average structure factors of the chains have been performed using different assumptions for chain disorder [24]. For instance, accordion motions with different amplitudes along $\boldsymbol{c}$ within a chain and with complete correlation between chains should produce diffuse streaks parallel to $\boldsymbol{c}^*$, which are not observed. Rotational motions of the chains around the $\boldsymbol{c}$ axis with no correlation between chains should also produce diffuse planes perpendicular to $\boldsymbol{c}^*$, but in this case, diffuse scattering is expected in the ($hk0$) plane, which does not agree with the experiments. Also when a torsional motion of the chain with correlation between chains is considered, diffuse streaks along $\boldsymbol{c}^*$ are predicted, which again is not consistent with the experimental results.

Thus, it can be safely concluded that the model of disordered translational displacements of the chain along $\boldsymbol{c}$ actually provides the best fit to the experimental data.

6.2.3. Correlation lengths. On the basis of the model of translational displacements of the chains, we have now to account for subtle additional phenomena, i.e. (i) the diffuse planes exhibit a finite width (figure 6), (ii) there are additional short modulations of the diffuse planes, giving rise to diffuse spots within each plane (figure 6). These phenomena are interpreted in terms of correlated short-range fluctuations.

In TMMC, if the chain were perfectly ordered along $\boldsymbol{c}$, i.e. if an infinite correlation length existed in the atomic displacements in that direction, then the diffuse planes would exhibit an infinitely small width. The observed width (figure 6) leads to a correlation length of about 18 unit cells along $\boldsymbol{c}$, which means that the chains are not completely ordered in that direction. In order words, each chain is made of ordered domains containing about 36 octahedra.

In addition to the intra-chain correlations, one also has to consider the existence of inter-chain correlations along the $\boldsymbol{a}$ or $\boldsymbol{b}$ directions, which are responsible for the presence

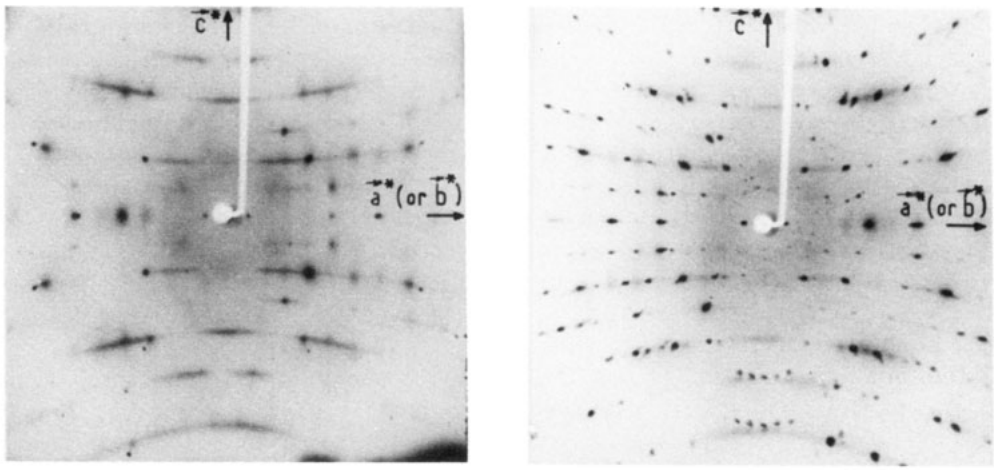

(a) (b)

Figure 9. Fixed-crystal photographs of the (a^*, c^*) or (b^*, c^*) plane of TMMC: (*a*) 150 K (phase I); (*b*) 113 K (phase II).

of a short modulation of the diffuse planes, appearing in the form of marked spots within each plane (figure 6). Then, short-range ordering phenomena exhibit some kind of three-dimensional character; from the size of the observed spots a^* or b^*, a correlation length of about six unit cells is measured, which means that the (a, b) planes in the direct lattice are made of ordered domains involving about 30 to 40 octahedra chains.

6.2.4. Temperature dependence of diffuse scattering. A preliminary study of the temperature dependence of the diffuse scattering in TMMC through the I ↔ II structural phase transition is presented in figure 9.

A lower temperature (150 K) in phase I, the diffuse scattering patterns (figure 9(*a*)) are essentially the same as those observed at room temperature (figure 6(*a*)), were it not for a noticeable narrowing of these patterns. Indeed, the width of the diffuse planes, which is related to intrachain correlation along c, diminishes significantly, which leads to an increase of the correlation length in the c direction from ≃18 unit cells at room temperature to ≃23 unit cells at 150 K. The inter-chain correlation length in the a or b direction also increases from ≃6 unit cells at room temperature to ≃8 to 9 unit cells at 150 K. These variations are attributed to premonitory effects of the I ↔ II transition at 126 K.

At lower temperature (113 K, figure 9(*b*)), the observation of superstructure Bragg peaks is a clear indication of the occurrence of phase II (see section 5). The diffuse scattering patterns are still observed, but their intensity is considerably lower than in phase I. As a matter of fact, phase II has been described as an ordered phase [5–8], and the remnant of scattering at 113 K (i.e. just below the transition temperature) is probably related to the presence of residual disorder, as was already evidenced for the TMA orientations in phase II at approximately the same temperature (see section 5).

Thus, the preliminary data suggest that the observed diffuse scattering is related to the fluctuations of the order parameter for the I ↔ II phase transition (see paper III).

However, critical scattering should not be very important close to the transition point, having regard to the rather strong first-order character of the phase change. In fact, extensive experiments very close to the transition temperature would be necessary to ascertain this point; such experiments are time-consuming and lie beyond the scope of the present study.

7. Conclusions

From the x-ray diffraction measurements reported in this paper, a number of important conclusions concerning the structural phase transitions occurring in TMMC and TMCC can be drawn:

(i) All structural modifications derive from a prototype structure (phase I') whose space group is $P6_3/mmc$ ($Z = 2$) and which exhibits orientational disorder of the TMA, of complex nature, involving at least 10 different orientations if a Frenkel-type description is adopted.

(ii) Phase I derives from phase I' by a rotation of the octahedra chains about the $\boldsymbol{c}$ axis. In the phase I the TMA are distributed between five different orientations pertaining to a combination of two models, with two and three potential wells, respectively.

(iii) Phase II is derived from phase I by antiphase translational displacements of the chains along $\boldsymbol{c}$. As far as x-ray diffraction measurements are concerned, the space group is determined as $P2_1/b$ ($Z = 4$), with a doubling of the lattice parameter along $\boldsymbol{b}$. Though phase II is expected to be ordered at low temperature, an important residual orientational disorder of the TMA persists just below the I $\leftrightarrow$ II transition temperature.

(iv) The space group of phase III is confirmed to be $P2_1/m$ ($Z = 2$).

(v) Phase IV exhibits a complex unit cell, derived from that of phase I by a trebling of the lattice constant along $\boldsymbol{c}$ and a doubling along $\boldsymbol{b}$; the space group is $P2_1/b$ ($Z = 12$).

The x-ray diffuse scattering patterns observed in phase I of TMMC and TMCC show the existence of chain disorder. A model is proposed, which fits nicely the experimental data; it consists of translational displacements of the octahedra chains along the $\boldsymbol{c}$ axis. The width of the observed diffuse planes is associated with intra-chain correlations in the atomic displacements; the corresponding correlation length is around 18 to 23 unit cells in the $\boldsymbol{c}$ direction, depending on temperature. The large modulations of the diffuse planes are assigned to the 'shape' factor of the inorganic chain, whereas the additional short modulations are attributed to the existence of inter-chain correlations; for these latter, a correlation length of 6 to 9 unit cells in the $\boldsymbol{a}$ or $\boldsymbol{b}$ direction is determined.

These results clearly show that structural disorder occurring in phase I of TMMC and TMCC concerns not only the orientation of the TMA groups but also the inorganic octahedra chains sublattice. The translational disorder of the chain probably has to be related to the existence of fluctuating potential wells for the TMA orientations, as evidenced from the structural determination.

In phase II of TMMC, a residual chain disorder is evidenced just below the I $\leftrightarrow$ II transition temperature, which again probably has to be related with a similar observation for the TMA orientation.

References

[1] Morosin B and Graeber E J 1967 *Acta Crystallogr.* **23** 766
[2] Morosin B 1972 *Acta Crystallogr.* B **28** 2303

[3] Peercy P S, Morosin B and Samara G A 1973 *Phys. Rev.* B **8** 3378
[4] Hutchings M T, Shirane G, Birgeneau R J and Holt S L 1972 *Phys. Rev.* B **5** 1999
[5] Mangun B W and Utton D B 1972 *Phys. Rev.* B **6** 2790
[6] Tsang T and Utton D B 1976 *J. Chem. Phys.* **64** 3780
[7] Mlik Y, Daoud A and Couzi M 1979 *Phys. Status Solidi* a **52** 175
[8] Mlik Y and Couzi M 1982 *J. Phys. C: Solid State Phys.* **15** 6891
[9] Hutchings M T, Pawley G S and Stirling W G 1983 *J. Phys. C: Solid State Phys.* **16** 115
[10] Couzi M and Mlik Y 1986 *J. Raman Spectrosc.* **17** 117
[11] Jewess M 1982 *Acta Crystallogr.* B **38** 1418
[12] Braud M N, Couzi M, Chanh N B, Meresse A, Hauw C and Gomez-Cuevas A 1990 *Ferroelectrics* **104** 367
[13] Lamcharfi T 1986 *Thesis* University of Bordeaux I (unpublished)
[14] Levola T and Laiho R 1986 *J. Phys. C: Solid State Phys.* **19** 6931
[15] Levola T and Laiho R 1988 *Solid State Commun.* **66** 557
[16] Tischenko G N 1955 *Tr. Inst. Kristallogr., Akad. Nauk SSSR* **11** 93
[17] Levola T and Kleemann W 1985 *Phys. Rev.* B **32** 4697
[18] Alcock N W and Holt S L 1978 *Acta Crystallogr.* B **34** 1970
[19] Sheldrick G 1976 *SHELX 76 System of Computing Programs* University of Cambridge
[20] *International Tables for X-ray Crystallography* 1974 vol IV (Birmingham: Kynoch)
[21] Mokhlisse R, Chanh N B, Couzi M, Haget Y, Hauw C and Meresse A 1984 *J. Phys. C: Solid State Phys.* **17** 233
[22] Négrier P, Couzi M, Chanh N B, Hauw C and Meresse A 1989 *J. Physique* **50** 405
[23] Guinier A 1964 *Théorie et Technique de la Radiocristallographie* (Paris: Dunod) p 506
[24] Braud M N 1989 *Thesis* University of Bordeaux I
[25] Denoyer F, Comes R, Lambert M and Guinier A 1974 *Acta Crystallogr.* A **30** 423